COMMUNICATION

Hierarchical tubular structures constructed from ultrathin TiO2(B) nanosheets for highly reversible lithium storage†

Han Hu,[a] Le Yu,[a] Xuehui Gao,[b] Zhan Lin*[b] and Xiong Wen (David) Lou*[a]

Hierarchical tubular structures constructed from TiO2(B) nanosheets were fabricated by an efficient Cu nanowire templated solvothermal method. A dense layer of TiO2(B) nanosheets was grown on the Cu nanowires during the initial stage of the reaction. The Cu nanowires were then gradually dissolved during the later stage of the prolonged reaction. The as-obtained TiO2(B) hierarchical tubes showed a large surface area and good shell permeability. When evaluated for electrochemical lithium storage properties, these TiO2(B) hierarchical tubular structures showed a high specific capacity, excellent rate performance and long-term cycling stability.

Owing to the fabulous architectures and tunable properties, hollow micro-/nanostructures have been demonstrated to have great potential in a myriad of applications, such as drug delivery, nanoreactors and energy storage and conversion devices.[1–9] Over the past few decades, numerous projects have been dedicated to developing reliable methods for the controllable synthesis of hollow structures with remarkable progress achieved.[2,3,5] In a normal templating method, removal of the templates by methods like etching in harsh solutions, calcination at high temperature or dissolution in organic solvents is simple in concept, however, practically it requires special care as deformation and collapse of the shells will otherwise occur.[3,10,11] In this regard, efficient syntheses of hollow structures with alternative templates that impose less influence on the shell materials when removed are highly desirable. For example, anatase TiO2 nanocages have been synthesized by templating against Cu2O polyhedral particles,

Broader context

Lithium ion batteries (LIBs) have become the dominant power source for portable electronics and have great potential to power electrical vehicles in the near future. To meet the requirements for use in high-power applications, battery electrodes that can deliver capacitor-like rate-performances are in high demand. TiO2(B) with favorable open channels allows lithiation/delithiation in an interesting pseudocapacitive manner. The electrochemical performance of TiO2(B) electrodes can be effectively enhanced by engineering nanostructures. However, TiO2(B) is a less stable phase and it is highly challenging to synthesize TiO2(B) electrode materials with desired nanostructures. In this work, we report the synthesis of hierarchical tubular structures constructed from TiO2(B) nanosheets through an efficient Cu nanowire templated solvothermal method. Benefiting from unique structural features, the as-obtained TiO2(B) hierarchical tubular structures show excellent electrochemical lithium storage properties with a high capacity, excellent rate capability and cycling stability.

which are conveniently eliminated by mild HCl etching while the shells remain intact.[12]

Titanium dioxide (TiO2) has been intensively studied as one of the most prominent anode materials for lithium-ion batteries (LIBs) because of the greatly improved safety and high rate capability.[13–16] Among all the polymorphs, TiO2(B) possesses favorable open channels, which facilitate lithiation/delithiation in an interesting pseudocapacitive manner, rather than the solid-state diffusion process observed in anatase TiO2.[17–21] As such, the theoretical capacity of TiO2(B) (335 mA h g^{-1}) is much higher than that of anatase TiO2 ($\sim$170 mA h g^{-1}), and comparable to the value of commercial graphite anodes.[22–24] Besides, theoretical and experimental studies have revealed a morphological dependence of the lithium insertion mechanism where the electrochemical lithium storage performance of TiO2(B) nanosheets growing along the *ab* plane is superior to that of other nanostructures such as nanowires, nanoparticles and nanobelts.[25] Motivated by the improved lithium storage capability of hollow structures with metal oxide nanosheets as building blocks,[26,27] hollow structures constructed from TiO2(B) nanosheets with a

[a] *School of Chemical and Biomedical Engineering, Nanyang Technological University, 62 Nanyang Drive, Singapore 637459. E-mail: xwlou@ntu.edu.sg, davidlou88@gmail.com; Web: http://www.ntu.edu.sg/home/xwlou/*

[b] *Institute of Chemical Engineering, College of Chemical and Biological Engineering, Zhejiang University, Hangzhou, Zhejiang, 310027, China. E-mail: zhanlin@zju.edu.cn*

large surface area and good shell permeability are highly anticipated to exhibit enhanced lithium storage properties. However, TiO$_2$(B) is a less stable phase of TiO$_2$ that will easily undergo irreversible phase transitions, which makes it difficult to construct TiO$_2$(B) hollow structures.[28] Thus, successful examples of hierarchical hollow structures constructed from TiO$_2$(B) nanosheets have not been reported previously to the best of our knowledge.

Herein, we report a template-engaged synthesis of hierarchical tubular structures constructed from TiO$_2$(B) nanosheets (denoted as TiO$_2$(B) HTs) through an efficient Cu nanowire templated solvothermal method. After initial deposition of the TiO$_2$(B) shells against the Cu nanowires, the Cu nanowires were simultaneously removed during the later stage of the solvothermal reaction. Thus, the influence on the shells during the template removing process has been minimized. When evaluated for lithium storage properties, these TiO$_2$(B) HTs showed a greatly enhanced electrochemical performance.

The synthesis strategy is schematically depicted in Fig. 1. In this method, highly uniform Cu nanowires with smooth surfaces (Fig. S1, see ESI†) synthesized by a hydrothermal process[29] were employed as templates. The Cu nanowires were first uniformly coated with a layer of TiO$_2$(B) through a solvothermal process with ethylene glycol as the solvent and TiCl$_3$ as the precursor.[30] By precisely controlling the reaction time, well-defined TiO$_2$(B) nanosheets were formed, giving rise to Cu@TiO$_2$(B) core–shell structures. Owing to their high reactivity, the Cu nanowires were gradually oxidized and removed in the acidic solution during the prolonged solvothermal treatment. During the whole process, the robust shells remained largely intact. As such, an interesting evolution from core–shell structures to hierarchical tubes could be observed with different solvothermal durations. The as-obtained TiO$_2$(B) HTs were further annealed in air to remove the organic species adsorbed on the nanosheets (Fig. S2, see ESI†) and also to improve the crystallinity at the same time.

The crystal structure of the as-prepared TiO$_2$(B) HTs was determined by X-ray diffraction (XRD). As shown in Fig. S3a (see ESI†), the peaks for (001), (110), (002) and (020) can be indexed to the TiO$_2$(B) phase (JCPDS card No. 46-1237).[31] On the other hand, the peaks associated with Cu (Fig. S1a, see ESI†) were
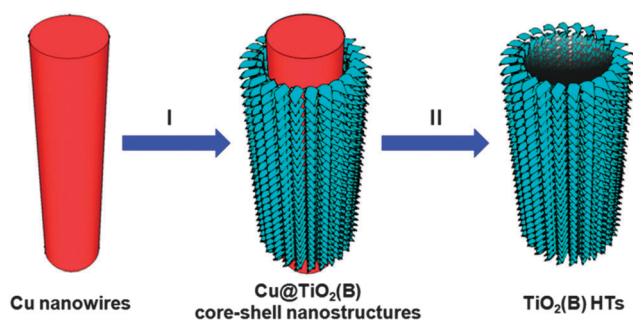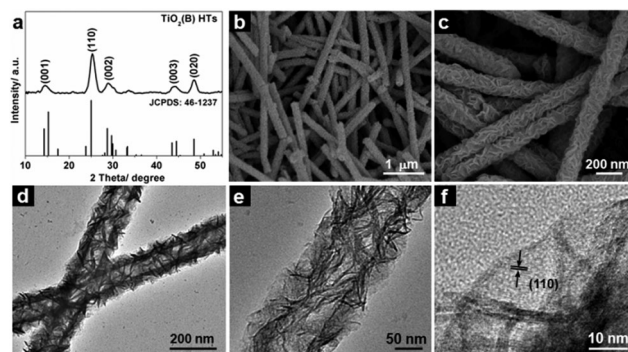

Fig. 2 XRD pattern (a), FESEM images (b, c), and TEM images (d–f) of the TiO$_2$(B) HTs after annealing at 350 °C for 2 h.

totally absent, indicating the complete removal of the templates, which was also confirmed by X-ray photoelectron spectroscopy (XPS) measurements (Fig. S4, see ESI†). The phase purity of the TiO$_2$(B) HTs was further supported by Raman spectrum (Fig. S3b, see ESI†) in which all the vibrational modes are in good agreement with previous studies on TiO$_2$(B).[28] After calcination, the organic species were fully removed (Fig. S5a, see ESI†) without deteriorating the phase purity, as confirmed by the XRD pattern shown in Fig. 2a. Panoramic field-emission scanning electron microscope (FESEM) images (Fig. 2b and Fig. S5b, see ESI†) show that the annealed product consisted entirely of uniform one-dimensional (1D) nanostructures. Compared to the original Cu nanowires (Fig. S1, see ESI†), both the surface roughness and diameter of these 1D nanostructures were increased significantly, indicative of the successful deposition of TiO$_2$(B) shells. The enlarged FESEM image (Fig. 2c) reveals that these 1D structures were constructed from randomly oriented nanosheets. Some broken shells in the FESEM images (Fig. 2c and Fig. S5c, see ESI†) reveal the hollow interior. The hollow interior was further examined by TEM. From the TEM images (Fig. 2d and e and Fig. S5d, see ESI†), the thickness of the shell was estimated to be around 50 nm. From the high-resolution TEM image in Fig. 2f, it can be clearly observed that the shell was constructed from nanosheets with a thickness of only a few nanometers. The d-spacing for the lattice fringe perpendicular to the sheet plane was determined to be about 0.36 nm, corresponding to the (110) lattice plane.[22,23] This observation indicates that the nanosheets grew along the ab plane as the growth along the c direction was hindered by the selectively adsorbed organic species.[22,23,28]

Time dependent experiments were conducted to investigate the structural evolution from Cu@TiO$_2$(B) core–shell structures to TiO$_2$(B) HTs. FESEM and TEM were used to characterize the products with different solvothermal durations. A uniform TiO$_2$(B) layer was formed after solvothermal treatment for 6 h (Fig. S6, see ESI†). However, well-defined nanosheets could only be observed with a duration longer than 9 h. As shown in Fig. 3a and Fig. S7 (see ESI†), a layer of TiO$_2$(B) nanosheets was uniformly coated on the Cu nanowires with a solvothermal duration of 9 h, producing core–shell structures. After that, there were little morphological changes observed in the TiO$_2$(B) shells from FESEM observations with solvothermal treatments

Fig. 1 Schematic illustration of the template-assisted formation of TiO$_2$(B) hierarchical tubes (TiO$_2$(B) HTs). (I) Deposition of TiO$_2$(B) nanosheets on Cu nanowires by a facile solvothermal process; (II) formation of TiO$_2$(B) HTs by prolonging the solvothermal treatment and subsequent annealing.

This journal is © The Royal Society of Chemistry 2015

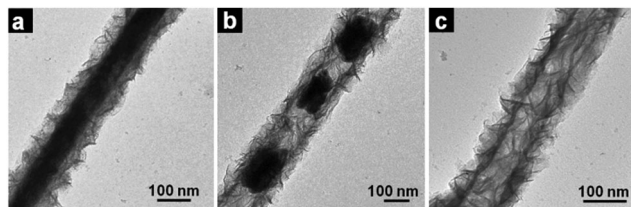Energy Environ. Sci., 2015, 8, 1480–1483 | 1481

Fig. 3 TEM images of the products with different solvothermal durations: (a) 9 h, (b) 12 h, (c) 24 h.

for up to 24 h (Fig. S7–S9, see ESI†). Nevertheless, TEM images reveal an interesting hollowing process where the interior cavities started to appear after reaction for 12 h (Fig. 3b) and the structure became fully hollow after reaction for 24 h (Fig. 3c), giving rise to the $TiO_2(B)$ HTs. The sequential processes of TiO_2 shell formation and selective Cu core removal may be associated with the different redox potentials of the Ti^{4+}/Ti^{3+} pair (-0.67 V vs. standard hydrogen electrode (SHE)) and Cu^+/Cu pair (0.52 V vs. SHE) or Cu^{2+}/Cu pair (0.337 V vs. SHE).[32,33] The Ti^{3+} species is more prone to oxidization, leading to the fast formation of $TiO_2(B)$ shells. On the other hand, the existence of Ti^{3+} may also protect the Cu core from being oxidized, which allows the $Cu@TiO_2$ core–shell structures to be preserved before the complete oxidation of Ti^{3+}. Afterwards, the Cu cores can be gradually oxidized by dissolved oxygen and the oxidized Cu will be quickly etched away in the acidic solution. It is interesting to note that the Cu nanowires were etched into discontinuous particles during the initial hollowing process (Fig. 3b). Finally, highly porous $TiO_2(B)$ HTs were formed, which exhibit a high surface area of 141 m^2 g^{-1} and porosity of 0.746 cm^3 g^{-1} (Fig. S10, see ESI†).

To evaluate the lithium storage performance of the annealed $TiO_2(B)$ HTs, various electrochemical measurements were carried out. Fig. 4a shows the cyclic voltammetry (CV) curves at a scan rate of 1.0 mV s^{-1}. The S peaks associated with pseudocapacitive lithium storage behaviour are quite distinctive in the potential range of 1.5–1.7 V, while the A peaks assigned to the solid-state lithium diffusion in anatase at 1.7/2.0 V are less pronounced. This observation indicates the high purity of the $TiO_2(B)$ phase and that the lithiation/delithiation processes mainly proceed in a pseudocapacitive manner.[22,23,34,35] Typical discharge–charge profiles of the $TiO_2(B)$ HTs at a current rate of 1 C (1 C = 335 mA g^{-1}) over a voltage window of 1–3 V are displayed in Fig. S11 (see ESI†). The initial discharge and charge capacities were 290 and 240 mA h g^{-1}, respectively. The unique architecture and high phase-purity endow the $TiO_2(B)$ HTs with a fast response to continuously varying current rates. As shown in Fig. 4b, high capacities of 216, 202, 182, 160 and 130 mA h g^{-1} can be delivered at current rates of 1, 2, 5, 10 and 20 C, respectively. After cycling at high rates, a capacity of 210 mA h g^{-1} can be restored when reducing the current rate back to 1 C (Fig. 4b and Fig. S12a, see ESI†). The electrochemical lithium storage performance of $TiO_2(B)$ nanospheres (NSs) synthesized under identical conditions except for the addition of Cu nanowires[28,30] (Fig. S13, see ESI†) was also evaluated. The capacities of these $TiO_2(B)$ NSs at low current rates were close to those of the $TiO_2(B)$ HTs,

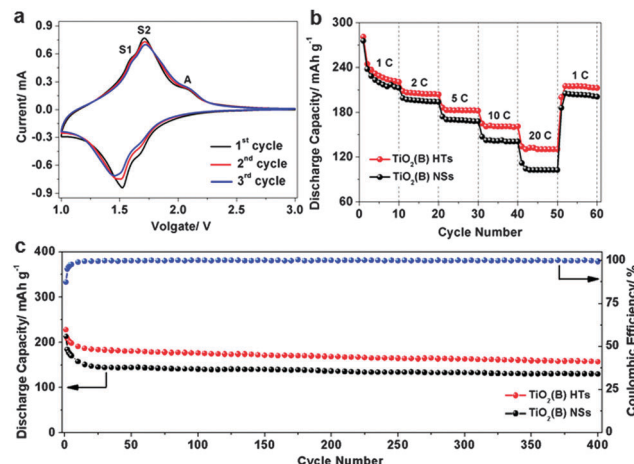**Fig. 4** (a) CV profiles of the $TiO_2(B)$ HTs showing the 1st, 2nd and 3rd cycles between 1.0 and 3.0 V at a scan rate of 1 mV s^{-1}. (b) Cycling performance of the $TiO_2(B)$ HTs and $TiO_2(B)$ NSs at different current rates. (c) Long-term cycling performance of the $TiO_2(B)$ HTs and $TiO_2(B)$ NSs at a constant current rate of 5 C and coulombic efficiency of the $TiO_2(B)$ HTs during the cycling process.

but much lower at high current rates (Fig. 4b and Fig. S12b, see ESI†). Moreover, the rate performance of the $TiO_2(B)$ HTs is superior to that of many previously reported $TiO_2(B)$ nanostructures (Fig. S14, see ESI†).[20,34,36,37] The cycling performance was tested for hundreds of cycles. Despite the decay in the initial few cycles, the capacity of the $TiO_2(B)$ HTs became stable and remained at 160 mA h g^{-1} after 400 cycles at a current rate of 5 C. This is superior to that of the $TiO_2(B)$ NSs (Fig. 4c and Fig. S15, see ESI†). A similar cycling performance was also demonstrated at a current rate of 10 C (Fig. S16, see ESI†). Electrochemical impedance spectroscopy (EIS) studies (Fig. S17, see ESI†) of the cells based on these two electrodes revealed that the $TiO_2(B)$ HTs showed a reduced diameter of the semicircle in the high-frequency region, indicative of lower resistance. Evidently, the superior electrochemical performance of the $TiO_2(B)$ HTs is related to the unique structural features. On the one hand, the porous shells constructed from randomly oriented nanosheets enlarge the electrolyte–electrode interface. The greatly reduced thickness of the nanosheets shortens the diffusion length for Li^+ ions, which allows faster lithiation/delithiation.[25,31] Furthermore, the interior cavities can efficiently accommodate the volume variation during the repeated lithium intake–extract processes. A post-mortem study revealed that the structure of these $TiO_2(B)$ HTs was largely retained after being discharged–charged over 400 cycles (Fig. S18, see ESI†). As such, these $TiO_2(B)$ HTs deliver excellent electrochemical lithium storage properties in terms of high capacity, good rate capacity and stable cycling performance.

In summary, an efficient template-assisted solvothermal method has been developed to synthesize $TiO_2(B)$ hierarchical tubular structures. The uniform deposition of $TiO_2(B)$ shells against Cu nanowires and the subsequent gradual dissolution of the Cu cores can be sequentially observed with different solvothermal durations. The as-prepared $TiO_2(B)$ hierarchical

1482 | Energy Environ. Sci., 2015, **8**, 1480–1483

This journal is © The Royal Society of Chemistry 2015

tubes were constructed from ultrathin nanosheets with a high surface area. Because of the unique structural features, these $TiO_2(B)$ hierarchical tubular structures deliver a high lithium storage capacity, remarkable rate performance and long-term cycling stability when evaluated as anodes for LIBs.

Notes and references

1 M. H. Oh, T. Yu, S. H. Yu, B. Lim, K. T. Ko, M. G. Willinger, D. H. Seo, B. H. Kim, M. G. Cho, J. H. Park, K. Kang, Y. E. Sung, N. Pinna and T. Hyeon, *Science*, 2013, **340**, 964.

2 X. Y. Lai, J. E. Halpert and D. Wang, *Energy Environ. Sci.*, 2012, **5**, 5604.

3 X. W. Lou, L. A. Archer and Z. C. Yang, *Adv. Mater.*, 2008, **20**, 3987.

4 J. Liu, H. Q. Yang, F. Kleitz, Z. G. Chen, T. Y. Yang, E. Strounina, G. Q. Lu and S. Z. Qiao, *Adv. Funct. Mater.*, 2012, **22**, 591.

5 J. Hu, M. Chen, X. S. Fang and L. W. Wu, *Chem. Soc. Rev.*, 2011, **40**, 5472.

6 Z. H. Dong, X. Y. Lai, J. E. Halpert, N. L. Yang, L. X. Yi, J. Zhai, D. Wang, Z. Y. Tang and L. Jiang, *Adv. Mater.*, 2012, **24**, 1046.

7 J. W. Nai, Y. Tian, X. Guan and L. Guo, *J. Am. Chem. Soc.*, 2013, **135**, 16082.

8 J. Liu, S. Z. Qiao, J. S. Chen, X. W. Lou, X. R. Xing and G. Q. Lu, *Chem. Commun.*, 2011, **47**, 12578.

9 J. B. Joo, M. Dahl, N. Li, F. Zaera and Y. D. Yin, *Energy Environ. Sci.*, 2013, **6**, 2082.

10 Z. Z. Yang, Z. W. Niu, Y. F. Lu, Z. B. Hu and C. C. Han, *Angew. Chem., Int. Ed.*, 2003, **42**, 1943.

11 S. S. Feng, W. Li, Q. Shi, Y. H. Li, J. C. Chen, Y. Ling, A. M. Asiri and D. Y. Zhao, *Chem. Commun.*, 2014, **50**, 329.

12 Z. Y. Wang and X. W. Lou, *Adv. Mater.*, 2012, **24**, 4124.

13 D. Deng, M. G. Kim, J. Y. Lee and J. Cho, *Energy Environ. Sci.*, 2009, **2**, 818.

14 X. F. Li and C. L. Wang, *J. Mater. Chem. A*, 2013, **1**, 165.

15 J. S. Chen, Y. L. Tan, C. M. Li, Y. L. Cheah, D. Y. Luan, S. Madhavi, F. Y. C. Boey, L. A. Archer and X. W. Lou, *J. Am. Chem. Soc.*, 2010, **132**, 6124.

16 Y. Zhao, X. F. Li, B. Yan, D. J. Li, S. Lawes and X. L. Sun, *J. Power Sources*, 2015, **274**, 869.

17 A. G. Dylla, G. Henkelman and K. J. Stevenson, *Acc. Chem. Res.*, 2013, **46**, 1104.

18 Y. Ren, Z. Liu, F. Pourpoint, A. R. Armstrong, C. P. Grey and P. G. Bruce, *Angew. Chem., Int. Ed.*, 2012, **51**, 2164.

19 H. S. Liu, Z. H. Bi, X. G. Sun, R. R. Unocic, M. P. Paranthaman, S. Dai and G. M. Brown, *Adv. Mater.*, 2011, **23**, 3450.

20 A. R. Armstrong, G. Armstrong, J. Canales, R. Garcia and P. G. Bruce, *Adv. Mater.*, 2005, **17**, 862.

21 A. R. Armstrong, G. Armstrong, J. Canales and P. G. Bruce, *Angew. Chem., Int. Ed.*, 2004, **43**, 2286.

22 S. H. Liu, H. P. Jia, L. Han, J. L. Wang, P. F. Gao, D. D. Xu, J. Yang and S. N. Che, *Adv. Mater.*, 2012, **24**, 3201.

23 S. H. Liu, Z. Y. Wang, C. Yu, H. B. Wu, G. Wang, Q. Dong, J. S. Qiu, A. Eychmuller and X. W. Lou, *Adv. Mater.*, 2013, **25**, 3462.

24 P. G. Bruce, B. Scrosati and J. M. Tarascon, *Angew. Chem., Int. Ed.*, 2008, **47**, 2930.

25 A. G. Dylla, P. H. Xiao, G. Henkelman and K. J. Stevenson, *J. Phys. Chem. Lett.*, 2012, **3**, 2015.

26 L. Zhang, G. Q. Zhang, H. B. Wu, L. Yu and X. W. Lou, *Adv. Mater.*, 2013, **25**, 2589.

27 J. X. Zhu, Z. Y. Yin, D. Yang, T. Sun, H. Yu, H. E. Hoster, H. H. Hng, H. Zhang and Q. Y. Yan, *Energy Environ. Sci.*, 2013, **6**, 987.

28 G. L. Xiang, Y. G. Wang, J. Li, J. Zhuang and X. Wang, *Sci. Rep.*, 2013, **3**, 1411.

29 M. Mohl, P. Pusztai, A. Kukovecz, Z. Konya, J. Kukkola, K. Kordas, R. Vajtai and P. M. Ajayan, *Langmuir*, 2010, **26**, 16496.

30 G. L. Xiang, T. Y. Li, J. Zhuang and X. Wang, *Chem. Commun.*, 2010, **46**, 6801.

31 V. Etacheri, J. E. Yourey and B. M. Bartlett, *ACS Nano*, 2014, **8**, 1491.

32 Z. Y. Wang, D. Y. Luan, S. Madhavi, C. M. Li and X. W. Lou, *Chem. Commun.*, 2011, **47**, 8061.

33 R. Nakamura, A. Okamoto, H. Osawa, H. Irie and K. Hashimoto, *J. Am. Chem. Soc.*, 2007, **129**, 9596.

34 C. Wessel, L. A. Zhao, S. Urban, R. Ostermann, I. Djerdj, B. M. Smarsly, L. Q. Chen, Y. S. Hu and S. Sallard, *Chem. – Eur. J.*, 2011, **17**, 775.

35 J. M. Li, W. Wan, H. H. Zhou, J. J. Li and D. S. Xu, *Chem. Commun.*, 2011, **47**, 3439.

36 J. Qu, J. E. Cloud, Y. A. Yang, J. N. Ding and N. Y. Yuan, *ACS Appl. Mater. Interfaces*, 2014, **6**, 22199.

37 H. Huang, J. W. Fang, Y. Xia, X. Y. Tao, Y. P. Gan, J. Du, W. J. Zhu and W. K. Zhang, *J. Mater. Chem. A*, 2013, **1**, 2495.

This journal is © The Royal Society of Chemistry 2015

Energy Environ. Sci., 2015, **8**, 1480–1483 | **1483**